

An optimal solid-shell finite element for modeling dielectric elastomers

Dana Bishara¹ and Mahmood Jabareen^{1*}

Micro Abstract

Dielectric elastomer (DE) based actuators are considered an emerging promising class of thin actuators, which may undergo large deformations and exhibit various modes of activation. For modeling DEs there is a need for a proper finite element technology for the numerical simulations, which captures their realistic response. A model that is calibrated to VHB will be presented, and an efficient low-order finite element that is able to tackle locking pathologies will be introduced.

¹Faculty of Civil & Environmental Engineering, Structural Engineering and Construction Management., Technion – Israel Institute of Technology, Haifa, Israel

*Corresponding author: cvjmah@technion.ac.il

Introduction

Electro-active polymers (EAPs) are an emerging class of soft active materials, which may experience large deformations when they are subjected to an external electric field. EAPs are inexpensive light-weight polymeric materials, therefore, they are considered ideal candidates for high performance low cost engineering applications. A typical actuator of EAPs consist of a thin film, which is sandwiched between two flexible electrodes coating its major surfaces. Applying an electric potential difference through the thickness, causes thinning of the film and lateral expansion [5]. These changes occur due to Coulomb forces between the opposite charges that accumulate on the major surfaces when an external field is applied.

Referring to the literature, several research groups have dedicated their work to profoundly study EAPs and provide efficient numerical tools. For instance, Steinmann's research group ([13], [10], [11], [12]) has developed variational principles and finite element formulations accounting for the electro-mechanical coupling. Moreover, Ask et al. ([1], [3], [2]) have studied the visco-elastic nature of the so called polyurethane using the standard Bubnov-Galerkin approach. Later, Ask et al. [4] have presented a volumetric locking free formulation, i.e., a mixed finite element formulation. Wissler and Mazza ([16], [15], [17], [14], [18]) have studied the so-called dielectric elastomer VHB, however in their works they have adopted a hyper-elastic behavior combined with the quasi-linear viscoelastic function.

Considering the aforesaid, there is a need of a computationally efficient finite element, which is able to eliminate possible locking pathologies and account for the visco-elastic behavior of EAPs. In this work, a solid-shell formulation is developed adopting both the assumed natural inhomogeneous strain method ANIS and the enhanced assumed strain method EAS. Furthermore, a strain energy function that accounts for the hyper-elastic

response, the viscoelastic response and the electromechanical coupling is presented.

1 Kinematics

In this section, both assumed natural inhomogeneous strain (ANIS) and enhanced assumed strain (EAS) concepts are introduced. For a convenient presentation, let $\boldsymbol{\xi} = [\xi_1, \xi_2, \xi_3]$ be the isoparametric coordinates, and $\{\xi_1, \xi_2\}$ be the inplane axes, while ξ_3 indicates the coordinate in the thickness direction. Thus, the reference and present covariant tangent vectors are $\left\{ \mathbf{G}_i = \frac{\partial \mathbf{X}}{\partial \xi_i}, \mathbf{g}_i = \frac{\partial \mathbf{x}}{\partial \xi_i} \right\}$, and the contravariant vectors are defined as $\left\{ \mathbf{G}^i = \frac{\partial \xi_i}{\partial \mathbf{X}}, \mathbf{g}^i = \frac{\partial \xi_i}{\partial \mathbf{x}} \right\}$. Now, using the covariant and contravariant basis vectors, the Green-Lagrange strain tensor \mathbf{E} is defined as

$$\mathbf{E} = \mathcal{E}_{ij} \mathbf{G}^i \otimes \mathbf{G}^j, \quad \mathcal{E}_{ij} = \frac{1}{2} (\mathbf{g}_i \cdot \mathbf{g}_j - \mathbf{G}_i \cdot \mathbf{G}_j). \quad (1)$$

The key idea behind the ANIS is to interpolate the transverse covariant inhomogeneous strain components, which are sampled in a given set of points placed on the element mid-plane to overcome the curvature thickness locking and the transverse shear locking. Specifically, the inhomogeneous strain tensor and its covariant components are given by

$$\mathbf{E}_{inh} = \mathbf{E} - \mathbf{E}_0, \quad \mathbf{E}_0 = \mathbf{E} (\xi_1 = 0, \xi_2 = 0, \xi_3 = 0), \quad \widehat{E}_{inh,ij} = \mathbf{E}_{inh} : (\mathbf{G}_i \otimes \mathbf{G}_j). \quad (2)$$

The components $\left\{ \widehat{E}_{inh,33}, \widehat{E}_{inh,13}, \widehat{E}_{inh,23} \right\}$ are evaluated in the sampling points and a bilinear interpolation is applied for modifying the covariant inhomogeneous transverse normal strain and a linear interpolation is applied for modifying the covariant inhomogeneous transverse shear strains (see [8]). The modified covariant inhomogeneous transverse strains will denoted as $\left\{ \widetilde{E}_{inh,33}, \widetilde{E}_{inh,13}, \widetilde{E}_{inh,23} \right\}$. Then, the modified inhomogeneous strain tensors is reconstructed as follows

$$\begin{aligned} \mathbf{E}_{inh}^{\text{ANIS}} &= \widehat{E}_{inh,11} (\mathbf{G}^1 \otimes \mathbf{G}^1) + \widehat{E}_{inh,12} (\mathbf{G}^1 \otimes \mathbf{G}^2 + \mathbf{G}^2 \otimes \mathbf{G}^1) \\ &+ \widehat{E}_{inh,22} (\mathbf{G}^2 \otimes \mathbf{G}^2) + \widetilde{E}_{inh,23} (\mathbf{G}^2 \otimes \mathbf{G}^3 + \mathbf{G}^3 \otimes \mathbf{G}^2) \\ &+ \widetilde{E}_{inh,33} (\mathbf{G}^3 \otimes \mathbf{G}^3) + \widetilde{E}_{inh,13} (\mathbf{G}^1 \otimes \mathbf{G}^3 + \mathbf{G}^3 \otimes \mathbf{G}^1), \end{aligned} \quad (3)$$

and the modified compatible strain tensor take the following form

$$\widetilde{\mathbf{E}}_c = \mathbf{E}_0 + \mathbf{E}_{inh}^{\text{ANIS}}. \quad (4)$$

For achieving a remedy for further possible locking phenomena, an additional tensor, which is also known as the enhanced assumed strain (EAS) tensor is added to the modified compatible strain tensor. Thus, the total strain tensor reads

$$\widetilde{\mathbf{E}} = \widetilde{\mathbf{E}}_c + \mathbf{E}^{enh} \quad (5)$$

2 Constitutive equations

In this section, we present the strain energy function, which has been considered for modeling EAPs. Referring to the work of [7], an invariant based strain energy function has been proposed, which lacks the effect of viscoelasticity. Using the Maxwellian ([6] and [9]) type rheological model of the isochoric response of the material consists of a single elastic branch representing the elastic ground network as well as viscous branches

each of them representing a single mobile viscous sub-network, the strain energy function can be extended to include the viscous branches. Thus, the total strain energy function is given by

$$\begin{aligned} \mathcal{W} = & \underbrace{\frac{K}{4} (J^2 - 1 - 2\ln(J)) + \sum_{i=1}^3 C_i (\bar{I}_1 - 3)^i}_{\mathcal{W}^{hyper}(\mathbf{C})}} - \underbrace{\frac{1}{2} J \epsilon_0 \epsilon_r \mathbf{C}^{-1} : (\mathbf{E} \otimes \mathbf{E})}_{\mathcal{W}^{coup}(\mathbf{C}, \mathbf{E})}} \\ & + \underbrace{\sum_{i=1}^n \frac{1}{2} \mu_i^v [\mathbf{C}' : \mathbf{A}_i - 3 - \ln(\det(\mathbf{A}_i))]}_{\mathcal{W}^{viscus}(\mathbf{C}, \mathbf{A}_1 \dots \mathbf{A}_n)} \end{aligned} \quad (6)$$

where $\{\mathbf{A}_1, \dots, \mathbf{A}_n\}$ are strain-like internal tensorial variables associated with the viscous Maxwell branches and $\{\mu_1^v, \dots, \mu_n^v\}$ are the viscous shear moduli of the branches. The evolution law of a single strain like internal variable is given by

$$\dot{\mathbf{A}}_i = \frac{1}{\tau_i^v} (\mathbf{C}'^{-1} - \mathbf{A}_i), \quad (7)$$

with $\{\tau_1^v, \dots, \tau_n^v\}$ are the relaxation times of the different Maxwell branches.

3 Variational principles

The functional of the total potential energy is expressed with the internal energy part due to the strain energy function, and to external part due to external tractions and electrical fluxes as the following

$$\Pi(\tilde{\mathbf{C}}, \mathbf{E}) = \Pi^{int} - \Pi^{ext} = \int_{\Omega_0} W(\tilde{\mathbf{C}}, \mathbf{E}) d\Omega_0 - \left[\int_{\partial\mathcal{B}_0^T} \mathbf{u} \cdot \bar{\mathbf{T}} d\Gamma_0 + \int_{\partial\mathcal{B}_0^Q} \phi \bar{Q} d\Gamma_0 \right] \quad (8)$$

where Ω_0 is the volume of the reference configuration. Applying Hu-Washizu multi-field variational principle, the variation of the internal potential energy is decomposed into two parts, one with respect to the modified right Cauchy-Green and the other with respect to the electric field,

$$\delta\Pi = \underbrace{\int_{\Omega_0} \tilde{\mathbf{S}} : \delta\tilde{\mathbf{E}}_c d\Omega_0}_{\delta\Pi_{\tilde{\mathbf{C}}}^{int,u}} + \underbrace{\int_{\Omega_0} \tilde{\mathbf{S}} : \delta\mathbf{E}^{enh} d\Omega_0}_{\delta\Pi_{\tilde{\mathbf{C}}}^{int,\alpha}} - \underbrace{\int_{\Omega_0} \mathbf{D} \cdot \delta\mathbf{E}}_{\delta\Pi_{\mathbf{E}}^{int}} - \delta\Pi^{ext} \quad (9)$$

where $\tilde{\mathbf{S}} = 2 \frac{\partial W}{\partial \tilde{\mathbf{C}}}$ is the second Piola-Kirchhoff evaluated within the modified $\tilde{\mathbf{C}} = 2\tilde{\mathbf{E}} + \mathbf{I}$, and $\mathbf{D} = -\frac{\partial W}{\partial \mathbf{E}}$ is the electric displacement vector. The internal variables controlling the enhanced strain field are determined from the fact that these internal variables are workless, $\delta\Pi_{\tilde{\mathbf{C}}}^{int,\alpha} = 0$. Finally, the linearizing of the variation takes the following form,

$$\begin{aligned} \Delta\delta\Pi^{int} = & \int_{\Omega_0} \left[\left(\Delta\tilde{\mathbf{E}}_c + \Delta\mathbf{E}^{enh} \right) : \tilde{\mathbf{C}}_{uu} : \delta\tilde{\mathbf{E}}_c + \tilde{\mathbf{S}} : \Delta\delta\tilde{\mathbf{E}}_c + \Delta\mathbf{E} \cdot \tilde{\mathbf{C}}_{u\phi} : \delta\tilde{\mathbf{E}}_c d\Omega_0 \right. \\ & \left. + \left(\Delta\tilde{\mathbf{E}}_c + \Delta\mathbf{E}^{enh} \right) : \tilde{\mathbf{C}}_{\phi u} \cdot \delta\mathbf{E} - \Delta\mathbf{E} \cdot \tilde{\mathbf{C}}_{\phi\phi} \cdot \delta\mathbf{E} \right] d\Omega_0 \end{aligned} \quad (10)$$

where $\tilde{\mathbf{C}}_{uu} = 4 \frac{\partial W}{\partial \tilde{\mathbf{C}} \partial \tilde{\mathbf{C}}}$ is the material tangent modulus tensor, $\tilde{\mathbf{C}}_{u\phi} = 2 \frac{\partial W}{\partial \tilde{\mathbf{C}} \partial \mathbf{E}}$ and $\tilde{\mathbf{C}}_{\phi u} = 2 \frac{\partial W}{\partial \mathbf{E} \partial \tilde{\mathbf{C}}}$ are the mixed derivatives third order tensors, and $\tilde{\mathbf{C}}_{\phi\phi} = -\frac{\partial W}{\partial \mathbf{E} \partial \mathbf{E}}$ is the electric displacement tangent tensor.

4 Numerical example

Adopting the parameters set that we have obtained in our previous research work for VHB, a numerical example is presented here. In this example, we consider a bimorph bending actuator of a bi-layered thin film. The actuator dimensions have been chosen as demonstrated in Fig. 2, where $L_1 = 20\text{mm}$, $L_2 = 5\text{mm}$ and $L_3 = 1\text{mm}$. The thickness consists of two thin layers, where each of them is 0.5mm thick. A coarse mesh of 10 elements in the length direction, 2 elements in the width and 2 elements in the thickness direction has been chosen as demonstrated in fig. 1.

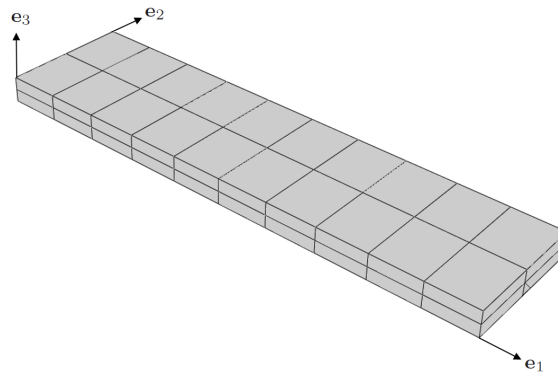


Figure 1. The coarse mesh that has been used for the simulation

The bottom layer is sandwiched between a pair of compliant electrodes located at the composite's bottom and in the mid plane on which potential differences can be applied, and the upper layer is electrically passive. Applying voltage causes a reduction in the thickness of the bottom layer, and at the same time, a lateral expansion. Since the active layer is perfectly adhered to the passive layer, the structure gradually bends towards the active layer.

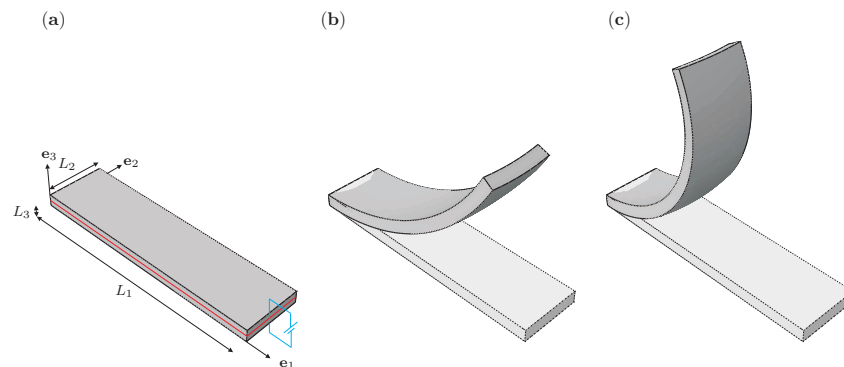


Figure 2. (a) The reference configuration of the actuator, $t=0$ sec. (b) The actuator at $t=50(\text{sec})$. (c) The current configuration of the actuator, $t=150$ sec.

The actuator is subjected to a voltage of 5kV , which is linearly ramped over a time period of 50 sec and followed by a constant value for 100 sec. Both horizontal and vertical displacements of a selected point A (the tip of the beam) were calculated and plotted in Fig. 3. When the linear voltage load is applied, i.e, $t \leq 50\text{sec}$, the actuator exhibits

highly nonlinear deformations. The actuator undergoes additional deformations due to creeping when the voltage is hold fix. As shown in Fig. 3, the additional displacements while creeping are not negligible, and this is because of the highly viscoelastic response of EAPs.

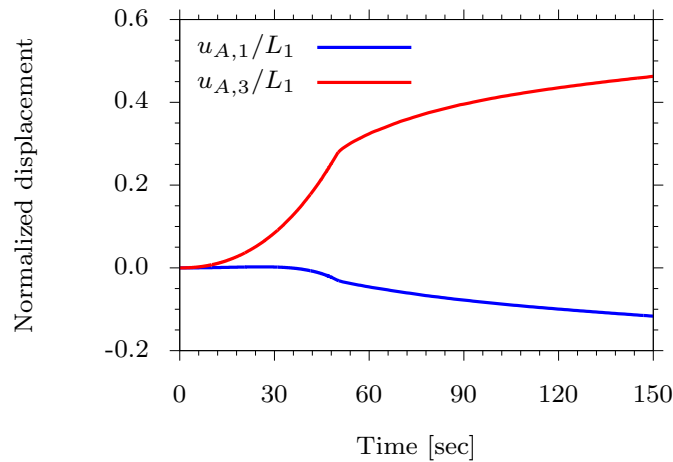


Figure 3. The normalized displacements, in both horizontal and vertical directions.

5 Conclusions

In this work, a numerical scheme accounting for the electro-mechanical coupling, the time-dependent response and the incompressibility has been developed for modelling EAPs. For this objective, the strain energy function has been split into a hyper-elastic term, a visco-elastic term and a coupling term. Following, a solid-shell finite element has been developed for avoiding several locking phenomena observed in thin structures. In summary, an efficient low order numerical tool has been developed in this work for modeling EAPs.

Acknowledgements

Financial support for this work was provided by the Israel Science Foundation under grant 1713/13, which is gratefully acknowledged.

References

- [1] A. Ask, A. Menzel, and M. Ristinmaa. On the modelling of electro-viscoelastic response of electrostrictive polyurethane elastomers. In *IOP Conference Series: Materials Science and Engineering*, volume 10, page 012101, 2010.
- [2] A. Ask, A. Menzel, and M. Ristinmaa. Electrostriction in electro-viscoelastic polymers. *Mechanics of Materials*, 50:9–21, 2012.
- [3] A. Ask, A. Menzel, and M. Ristinmaa. Phenomenological modeling of viscous electrostrictive polymers. *International Journal of Non-Linear Mechanics*, 47(2):156–165, 2012.
- [4] A. Ask, A. Menzel, and M. Ristinmaa. Inverse-motion-based form finding for quasi-incompressible finite electroelasticity. *International Journal for Numerical Methods in Engineering*, 94(6):554–572, 2013.

- [5] J. Blok and D. Legrand. Dielectric breakdown of polymer films. *Journal of Applied Physics*, 40(1):288–293, 1969.
- [6] M. Green and A. Tobolsky. A New Approach to the Theory of Relaxing Polymeric Media. *The Journal of Chemical Physics*, 14:80–92, 1946.
- [7] M. Jabareen. On the Modeling of Electromechanical Coupling in Electroactive Polymers Using the Mixed Finite Element Formulation. *Procedia IUTAM*, 12:105–115, 2015.
- [8] M. Jabareen and E. Mtanes. A solid-shell Cosserat point element (SSCPE) for elastic thin structures at finite deformation. *Computational Mechanics*, 2:1–31, 2016.
- [9] J. Lubliner. A model of rubber viscoelasticity. *Mechanics Research Communications*, 12(2):93–99, 1985.
- [10] D. Vu and P. Steinmann. Material and Spatial Motion Problems in Nonlinear Electro- and Magneto-elastostatics. *Mathematics and Mechanics of Solids*, 15:239–257, 2010.
- [11] D. Vu and P. Steinmann. On 3-D coupled BEM-FEM simulation of nonlinear electro-elastostatics. *Computer Methods in Applied Mechanics and Engineering*, 201-204:82–90, 2012.
- [12] D. Vu and P. Steinmann. On the spatial and material motion problems in nonlinear electro-elastostatics with consideration of free space. *Mathematics and Mechanics of Solids*, 17(8):803–823, 2012.
- [13] D. Vu, P. Steinmann, and G. Possart. Numerical modelling of non-linear electroelasticity. 70:685–704, 2007.
- [14] M. Wissler. *Modelling dielectric elastomer actuators*. PhD thesis, Swiss federal institute of technology in Zurich, 2007.
- [15] M. Wissler and E. Mazza. Modeling and simulation of dielectric elastomer actuators. *Smart Materials and Structures*, 14:1396–1402, 2005.
- [16] M. Wissler and E. Mazza. Modeling of a pre-strained circular actuator made of dielectric elastomers. *Sensors and Actuators A*, 120:184–192, 2005.
- [17] M. Wissler and E. Mazza. Electromechanical coupling in dielectric elastomer actuators. *Sensors and Actuators A*, 138:384–393, 2007.
- [18] M. Wissler and E. Mazza. Mechanical behavior of an acrylic elastomer used in dielectric elastomer actuators. *Sensors and Actuators, A: Physical*, 134(2):494–504, 2007.